

Constraints on the abundance of massive primordial black holes from lensing of compact radio sources

HUAN ZHOU,¹ ZHENGXIANG LI,² SHUO CAO,² AND ZHIQI HUANG¹

¹*School of Physics and Astronomy, Sun Yat-sen University, Zhuhai, 519082, China*

²*Department of Astronomy, Beijing Normal University, Beijing 100875, China*

ABSTRACT

The possibility that primordial black holes (PBHs) form a part of dark matter has been considered over a wide mass range from the Planck mass (10^{-5} g) to the level of the supermassive black hole in the center of the galaxy. Primordial origin might be one of the most important formation channel of massive black holes. We propose the lensing effect of very long baseline interferometer observations of compact radio sources with extremely high angular resolution as a promising probe for the presence of intergalactic PBHs in the mass range $\sim 10^2$ - $10^9 M_{\odot}$. For a sample of well-measured 543 compact radio sources, no millilensing multiple images are found with angular separations between 0.2 milliarcsecond and 50 milliarcseconds. From this null search result, we derive that the fraction of dark matter made up of PBHs in the mass range $\sim 10^4$ - $10^8 M_{\odot}$ is $\lesssim 0.56\%$ at 68% confidence level.

Keywords: Massive primordial black holes, Compact radio sources, Gravitational lensing

1. INTRODUCTION

The cosmological constant plus cold dark matter (Λ CDM) model has explained the evolution of the universe successfully. The scenario where CDM accounts for about a quarter of the total energy density is well consistent with current cosmological observations. However, we still know little about the constituent of dark matter (DM). Primordial black holes (PBHs) (Hawking 1971; Carr & Hawking 1974; Carr 1975), which are predicted to form in the infant universe via different mechanisms, such as the enhanced curvature perturbations during inflation (Clesse & García-Bellido 2015; Pi et al. 2018; Ashoorioon et al. 2019; Fu et al. 2019; Chen & Cai 2019; Motohashi et al. 2020), bubble collisions (Hawking et al. 1982), cosmic string (Hogan 1984; Hawking 1989), and domain wall (Caldwell et al. 1996), have been considered to be a promising candidate for the long elusive missing DM and therefore been a source of interest for nearly half a century. More interestingly, (stellar mass) PBHs have been attracting particular attention since the first detection of gravitational wave (GW) signal from the merger of black hole binary (Abbott et al. 2016).

This signal also can be interpreted as ripples of space-time from the merger of PBH binary (Bird et al. 2016; Sasaki et al. 2016; Clesse & García-Bellido 2017a).

So far, numerous methods have been proposed to constrain the abundance of PBHs, usually quoted as the fraction of PBHs in DM $f_{\text{PBH}} = \Omega_{\text{PBH}}/\Omega_{\text{DM}}$ at present universe, in various possible mass windows including direct observational effects: gravitational lensing (Kasziola et al. 1991; Alcock et al. 2001; Wilkinson et al. 2001; Tisserand et al. 2007; Griest et al. 2013; Mediavilla et al. 2017; Zumalacarregui & Seljak 2018; Nikura et al. 2019,a; Liao et al. 2020; Zhou et al. 2021), dynamical effects on ultrafaint dwarf galaxies (Brandt 2016; Koushiappas & Loeb 2017), disruption of white dwarfs (Graham et al. 2015), the effect of accretion via cosmic microwave background observations (Chen et al. 2016; Ali-Haimoud et al. 2017; Aloni et al. 2017; Poulin et al. 2017; Bernal et al. 2017), nondetections of stochastic GW from binary black holes (Clesse & García-Bellido 2017b; Wang et al. 2018; Chen & Huang 2020; De Luca et al. 2020; Gert, et al. 2020), (extra)galactic γ -ray backgrounds (Carr et al. 2016; DeRocco & Graham 2019; Laha 2019; Laha et al. 2020), and indirect observational effects: null detection of scalar-induced GW (Chen et al. 2019), cosmic microwave background (CMB) spectral distortions from the primordial density perturbations (Carr & Lidsey 1993; Carr et al. 1994). In addi-

zxli918@bnu.edu.cn

caoshuo@bnu.edu.cn

tion to these available probes, some other constraints from the near future observations, such as gravitational lensing of GW (Diego 2020; Liao et al. 2020), gamma-ray bursts (Ji et al. 2018), and 21 cm signals (Hektor et al. 2018; Clark et al. 2018; Halder & Banerjee 2020), have been proposed. See Sasaki et al. (2018); Green & Kavanagh (2020) for a recent review.

In addition to stellar or much smaller mass ranges, PBHs are also appealing for investigating the issue of supermassive black holes (SMBHs) observed at very high redshifts. For instance, observations of quasars at $z \geq 6$ indicate that SMBH with masses greater than $\sim 10^9 M_\odot$ (Yang et al. 2020), which are challenging to be formed via some astrophysical processes (Woods et al. 2019). That is, the formation mechanism of SMBH is still a mystery in astrophysics. Actually, even assuming that the black hole continues the Eddington-limited accretion, it is nearly impossible for stellar-mass black holes ($\sim 10 - 1000 M_\odot$) growing to reach the mass of $\sim 10^9 M_\odot$ during the lifetime of the universe at $z \simeq 6$. Moreover, it is also not yet clear if such an efficient accretion can persistently operate for cases from stellar-mass BHs to SMBHs within the Hubble time. Therefore, PBHs as progenitor of SMBHs are an alternative possibility and have been widely studied in the literature (Duechting 2004; Kawasaki et al. 2012; Nakama et al. 2016; Hasegawa & Kawasaki 2018; Kawasaki & Murai 2019; Kitajima & Takahashi 2020). However, it is known that if PBHs with masses $10^4 - 10^{13} M_\odot$ are assumed to originate from the Gaussian primordial curvature perturbation, such primordial perturbations ineluctably result in the spectral distortion of the CMB which significantly exceeds the upper limit obtained by the COBE/FRIAS experiment (Kohri et al. 2014). Therefore, a scenario with highly non-Gaussian perturbations has been proposed to create PBHs (Kohri et al. 2014; Nakama et al. 2016; Huang 2019; Shinohara et al. 2020). This formation mechanism predicts inevitable clustering of PBHs. In this case, direct probe for PBHs in the mass range $\sim 10^2 - 10^9 M_\odot$ using the lensing effect of very long baseline interferometer (VLBI) observations of compact radio source (CRS) with extremely high angular resolution would be a crucial test of the scenario where PBHs can explain SMBHs at high redshifts.

In this paper, we first apply the method of optical depth to constrain the abundance of PBHs with well-measured 543 CRSs, observed by a well-known VLBI survey undertaken by Preston et al. (1985) (hereafter P85). Benefit from the high-quality maps obtained by VLBI, one is able to measure the milliarcsecond ultra-compact structure in radio sources (Kellermann 1993) and search possible examples of multiple imaging pro-

duced by millilensing. Based on the the null search result with updated redshift measurements of P85 (Jackson & Jannetta 2006), we obtain the most stringent limit on the abundance of massive PBHs in the mass range $\sim 10^4 - 10^8 M_\odot$.

This paper is organized as follows: we introduce the CRS data and the theory of optical depth of CRS lensing in Section 2. In section3, we apply this method to the CRS observations and yield results. Conclusions and discussions are presented in Section 4. Throughout, we use the concordance Λ CDM cosmology with the best-fit parameters from the recent Planck observations (Planck Collaboration, 2020).

2. METHOD

In this section, we briefly introduce current data of CRS observations and the optical depth theory of CRS lensing.

2.1. Compact Radio Source Observations

The parent data used in this paper was derive from a catalog of ultra-compact radio sources, based on the observations of a 2.29 GHz VLBI all-sky survey (Preston et al. 1985). By employing a intercontinental VLBI array with an effective baseline of $\sim 8 \times 10^7$ wavelengths, 917 sources have been systematically observed with compact structure out of 1398 known radio sources. Note that these detected extragalactic objects coincide with different optical counterparts such as BL Lac objects, quasars, and radio galaxies (Gurvits 1994; Gurvits, Kellerman & Frey 1999; Cao et al. 2015), with a correlated flux limit of approximately 0.1 Jy. In this analysis, we focus on the a revised sample including a significant fraction of P85 catalog, with updated redshift measurements and radio information for 613 objects covering the redshift range of $0.0035 \leq z \leq 3.787$. The full description of the observations and the corresponding details (i.e., source name, angular size of the compact structure, total radio flux density, spectral index, and optical counterpart) can be found in (Preston et al. 1985; Jackson & Jannetta 2006)¹. Such data has been extensively investigated in a number of cosmological studies, focusing on its possibility of establishing a sample of standard cosmological rulers at higher redshifts (Jackson 2004; Cao et al. 2017a,b, 2018; Qi et al. 2019, 2021). On the other hand, it is well known that radio-loud active galactic nuclei (AGN) typically contains a flat-spectrum core and a steep-spectrum jet. In the framework of core-jet model proposed by Blandford & Königl (1979), flat-spectrum radio sources could be explained as the sta-

¹ A full list is available via <http://nrl.northumbria.ac.uk/13109/>.

tionary compact ends of quasi-steady supersonic jets, which always appear as the brightest unresolved compact cores in the VLBI images. Therefore, following the analysis of Gurvits, Kellerman & Frey (1999), we also apply a selection criterion to define the so-called "flat-spectrum core", with spectral index $\alpha \geq -0.5$. In this context, the spectra index is defined as $S \propto \nu^\alpha$, where S is the flux density and ν is the frequency. The redshift distribution for the final CRS sample ($N = 543$), which contains all of the strongest flat-spectrum compact radio sources in P85 VLBI survey, is shown in Fig. 1.

Presence of two or more flat-spectrum core images provides a simple and interesting probe to detect candidates of lensed CRSs, with massive PBHs acting as point-like lenses. We try to find suitable lens candidates from the 543 flat-spectrum CRSs, based on the three selection criteria as mentioned in Wilkinson et al. (2001): I) For the surface-brightness distribution of CRS, the primary compact component should be much larger than the secondary and other counterparts; II) For the flux density the CRS cores, the ratio of the primary and secondary compact components should be $\leq 40 : 1$; III) For the positions of the CRS cores, the separation of the primary and secondary compact components should be $\delta \leq \Delta\theta \leq \Delta$. Here δ and Δ denote the minimum and maximum image separations, i.e., the angular resolution and the limited field of view (FoV) of the observation with which each radio source was observed. The first quantity which needs clarification is the achievable resolution with the visibility distribution of the VLBI core. Given the mean angular size of the P85 radio sources (~ 1.5 mas), such issue has been extensively discussed in the literature, based on the resolution criteria focusing on the minimum resolvable size of a Gaussian component (Lobanov et al. 2005; Kovalev et al. 2005)

$$\theta_{\text{lim}} = b \left[\frac{4 \ln 2}{\pi} \ln \left(\frac{SNR}{SNR - 1} \right) \right]^{1/2}. \quad (1)$$

More specifically, with the representative value for the half-power beam width (b) and the signal-to-noise ratio (SNR) from P85 survey, the corresponding resolution is $\theta_{\text{lim}} \sim 0.20$ mas with a baseline $B = 8 \times 10^7$ (Jackson 2012), which can be significantly smaller than the typical value used in the previous works (Wilkinson et al. 2001). The second quantity we clarify is the FoV within which each radio source was observed. In this analysis we make a conservative estimation and take the typical value of $\Delta = 50$ mas.

After a careful check of the final CRS sample, all of the 543 flat-spectrum CRSs are excluded from lensed candidates, due to the one or a combination of selection criteria above. Therefore, no strong evidence of

millilensed candidate is found. Now such null search result will be used to place quantitative limits on the abundance of massive PBHs in the Universe.

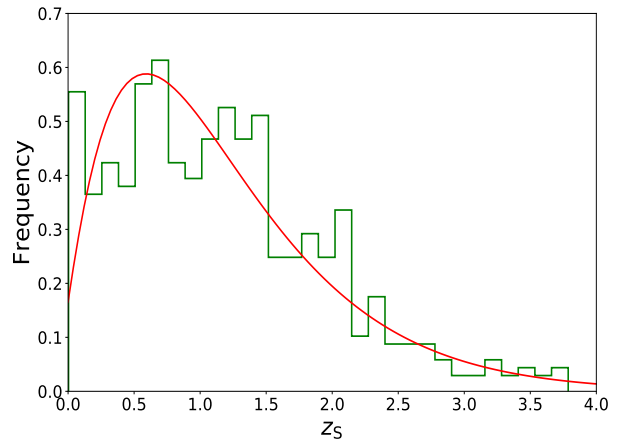


Figure 1. Redshift distribution of well-measured 543 CRSs.

2.2. Lensing of Compact Radio Sources

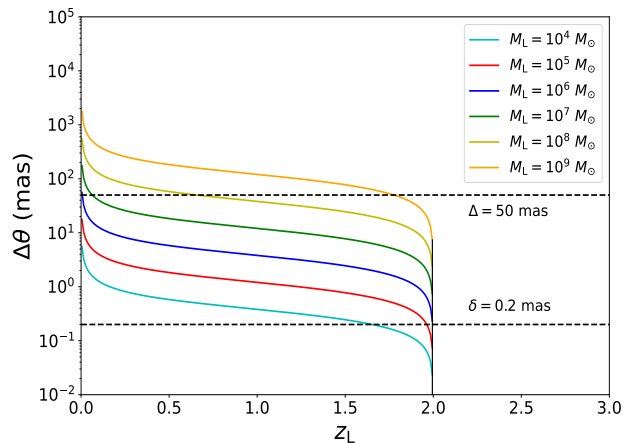


Figure 2. The angular separation of two images as a function with respect to the redshift of the lens, for a source at redshift $z_S = 2$. The mass of the lens ranges from 10^4 to $10^9 M_\odot$. The magnifications ratio of the images is $R_f = 40$.

For a point mass M_{PBH} lens, Einstein radius is

$$\theta_E = 2 \sqrt{\frac{GM_{\text{PBH}}}{c^2 D}} \approx (1 \text{ mas}) \left(\frac{M_{\text{PBH}}}{10^5 M_\odot} \right)^{1/2} \left(\frac{D}{\text{Gpc}} \right)^{-1/2}, \quad (2)$$

where G and c denote the gravitational constant and the speed of light, respectively. In addition, $D = D_L D_S / D_{LS}$ is effective lensing distance, where D_S , D_L ,

and D_{LS} represent the angular diameter distance to the source, to the lens, and between the source and the lens, respectively. The angular resolution for some CRSs with VLBA could reach a high level, e.g. $\sim \text{mas}$ of VLBA observations, it is possible to distinguish multiple images of an CRS lensed by intervening objects with mass greater than $\sim 10^5 M_\odot$. Because the Schwarzschild radius of PBH is much smaller than the Einstein radius multiplied by the angular diameter distance of the lens, i.e. $R_{\text{PBH}} = 2GM_{\text{PBH}}/c^2 \ll \theta_{\text{E}} D_{\text{L}}$, the lens equation of a point mass M_{PBH} is

$$\theta^2 - \beta\theta - \theta_{\text{E}}^2 = 0, \quad (3)$$

where β stands for the source position. The above lens equation of a point mass lens means there would be two images at positions

$$\theta_{\pm} = \frac{1}{2} \left(\beta \pm \sqrt{\beta^2 + 4\theta_{\text{E}}^2} \right). \quad (4)$$

It is obvious that one image locates outside the Einstein ring with $\theta_+ > \theta_{\text{E}}$ and the other one is within the ring $\theta_- < \theta_{\text{E}}$. Their magnifications μ_{\pm} satisfy

$$\mu_{\pm} = \left(1 - \frac{\theta_{\text{E}}^4}{\theta_{\pm}^4} \right)^{-1}. \quad (5)$$

In addition, the magnification ratio between two images can be directly obtained as well,

$$R_{\text{f}} \equiv \left| \frac{\mu_+}{\mu_-} \right| = \left| \frac{\theta_+}{\theta_-} \right|^4, \quad (6)$$

where the relation between two images $\theta_+ \theta_- = -\theta_{\text{E}}^2$ is used. The normalized impact parameter $y \equiv \frac{\beta}{\theta_{\text{E}}}$ for a reference value of magnification ratio R_{f} is

$$y(R_{\text{f}}) = R_{\text{f}}^{1/4} - R_{\text{f}}^{-1/4}. \quad (7)$$

In order to make both lensed images, especially the fainter one, detectable with high enough signal-noise ratio, R_{f} should be smaller than a threshold $R_{\text{f,max}}$. Accordingly, the impact parameter would be smaller than a certain value $y_{\text{max}}(R_{\text{f,max}}) = R_{\text{f,max}}^{1/4} - R_{\text{f,max}}^{-1/4}$. Following [Wilkinson et al. \(2001\)](#), we set the maximum value of magnification ratio $R_{\text{f,max}} = 40$.

The lensing cross section due to a PBH lens is given by

$$\sigma(M_{\text{PBH}}, z_{\text{L}}, z_{\text{S}}) = \frac{4\pi G M_{\text{PBH}} D_{\text{L}} D_{\text{LS}}}{c^2 D_{\text{S}}} [y_{\text{max}}^2(\Delta, M_{\text{PBH}}, z_{\text{L}}, z_{\text{S}}) - y_{\text{min}}^2(\delta, M_{\text{PBH}}, z_{\text{L}}, z_{\text{S}})], \quad (8)$$

where the maximum impact parameter $y_{\text{max}}(\Delta, M_{\text{PBH}}, z_{\text{L}}, z_{\text{S}})$ and minimum impact parameter $y_{\text{min}}(\delta, M_{\text{PBH}}, z_{\text{L}}, z_{\text{S}})$ are determined by the angular

resolution δ and the FoV of the observation Δ , respectively. Meanwhile, the impact parameter must be smaller than $y_{\text{max}}(R_{\text{f,max}})$. Now, we explain the maximum and minimum impact parameter in the cross section. The angular separation of two images lensed by a PBH is

$$\Delta\theta = \theta_{\text{E}}(R_{\text{f}}^{1/4} + R_{\text{f}}^{-1/4}). \quad (9)$$

Illustratively, as shown in Fig 2, for an CRS at redshift $z_{\text{S}} = 2$, imaged with a fixed $R_{\text{f}} = 40$, $\delta = 0.2 \text{ mas}$, and $\Delta = 50 \text{ mas}$, we have plotted the angular separation of the images against the redshift of the lens with different masses. It is obvious that the angular separation $\Delta\theta$ decreases as lens redshift z_{L} increases. For a source at $z_{\text{S}} = 2$ and small mass PBH lenses ($\lesssim 10^5 M_\odot$), the upper limit of the lens redshift producing two detectable images is truncated by the angular resolution δ (the lower dotted line in Fig. 2). While for large mass PBH lenses ($\gtrsim 10^7 M_\odot$), the lower limit of the lens redshift producing two detectable images is determined by the FoV Δ (the upper dotted line in Fig. 2). It is obvious that the upper bound of lens redshift is very close to the one of the source and lower bound is very close to zero within the mass range $10^5 \sim 10^7 M_\odot$.

If the angular resolution is δ , we only are able to detect the presence of lens mass M_{PBH} assuming an CRS is at redshift z_{S} when the value of angular separation of two images satisfy

$$\Delta\theta \geq \delta. \quad (10)$$

This requirement results in a minimum impact parameter $y_{\text{min}}(\delta, M_{\text{PBH}}, z_{\text{L}}, z_{\text{S}})$. Analogously, we can only detect secondary images if they lie within the FoV of the observation, Δ . That is, the value of angular separation of two images must satisfy

$$\Delta\theta \leq \Delta. \quad (11)$$

This condition yields a maximum impact parameter $y_{\text{max}}(\Delta, M_{\text{PBH}}, z_{\text{L}}, z_{\text{S}})$. For a given lens mass M_{PBH} and an CRS at redshift z_{S} , Eq. 11 will always be violated when the redshift of lens is smaller than z_{Δ} , a solution of $\Delta\theta = 2\theta_{\text{E}} = \Delta$. This violation heralds that the minimum angular separation of two images is larger than the FoV of the observation. Therefore, there is no contribution of cross section at redshifts smaller than z_{Δ} . Moreover, when the redshift of lens is between z_{Δ} and z_{δ} that comes from the $\Delta\theta = 2\theta_{\text{E}} = \delta$, the minimum angular separation of two images come in the range of FoV but is still larger than the angular resolution. In this case, the minimum impact parameter $y_{\text{min}}(\delta, M_{\text{PBH}}, z_{\text{L}}, z_{\text{S}})$ must be zero. However, the maximum impact parameter $y_{\text{max}}(\Delta, M_{\text{PBH}}, z_{\text{L}}, z_{\text{S}})$ can be

derived from Eq. 11 as follows

$$y_{\max}(\Delta, M_{\text{PBH}}, z_{\text{L}}, z_{\text{S}}) = \frac{\Delta/\theta_{\text{E}} + \sqrt{(\Delta/\theta_{\text{E}})^2 - 4}}{2} \frac{2}{\Delta/\theta_{\text{E}} + \sqrt{(\Delta/\theta_{\text{E}})^2 - 4}}. \quad (12)$$

When the redshift of lens is larger than z_{δ} , the minimum impact parameter $y_{\min}(\delta, M_{\text{PBH}}, z_{\text{L}}, z_{\text{S}})$ can be derived Eq. 9 as

$$y_{\min}(\delta, M_{\text{PBH}}, z_{\text{L}}, z_{\text{S}}) = \frac{\delta/\theta_{\text{E}} + \sqrt{(\delta/\theta_{\text{E}})^2 - 4}}{2} \frac{2}{\delta/\theta_{\text{E}} + \sqrt{(\delta/\theta_{\text{E}})^2 - 4}}. \quad (13)$$

It should be pointed out that the method in [Kassiola et al. \(1991\)](#) for calculating the truncated redshifts leads to underestimate of cross section contribution from the low redshift and the redshift close to the source. Therefore, for a single source, the lensing optical depth due to a single PBH lens should be

$$\begin{aligned} \tau(M_{\text{PBH}}, f_{\text{PBH}}, z_{\text{S}}) &= \int_0^{z_{\text{S}}} d\chi(z_{\text{L}})(1+z_{\text{L}})^2 n_{\text{L}}(f_{\text{PBH}}) \\ \sigma(M_{\text{PBH}}, z_{\text{L}}, z_{\text{S}}) &= \frac{3}{2} f_{\text{PBH}} \Omega_{\text{DM}} \int_0^{z_{\text{S}}} dz_{\text{L}} \frac{H_0^2}{cH(z_{\text{L}})} \frac{D_{\text{L}} D_{\text{LS}}}{D_{\text{S}}} \\ (1+z_{\text{L}})^2 [y_{\max}^2(\Delta, M_{\text{PBH}}, z_{\text{L}}, z_{\text{S}}) - y_{\min}^2(\delta, M_{\text{PBH}}, z_{\text{L}}, z_{\text{S}})], \end{aligned} \quad (14)$$

where n_{L} is the comoving number density of the lens, H_0 is the Hubble constant, $H(z_{\text{L}})$ is the Hubble parameter at z_{L} , and Ω_{DM} is the present fractional density of DM.

Now, for a given distribution function $N(z_{\text{S}})$ of CRSs, their integrated optical depth $\bar{\tau}(M_{\text{PBH}}, f_{\text{PBH}})$ is

$$\bar{\tau}(M_{\text{PBH}}, f_{\text{PBH}}) = \int dz_{\text{S}} \tau(M_{\text{PBH}}, f_{\text{PBH}}, z_{\text{S}}) N(z_{\text{S}}). \quad (15)$$

If one observes a large number of CRSs, N_{CRS} , then the number of detectable lensed CRSs is expected to be

$$N_{\text{lensed CRS}} = (1 - e^{-\bar{\tau}(M_{\text{PBH}}, f_{\text{PBH}})}) N_{\text{CRS}}. \quad (16)$$

If none of the CRS is found to be lensed, then the constraint on the upper limit of the fraction of DM in the form of PBHs can be estimated from Eq. 16.

3. RESULTS

We first use the optical depth method to constrain the abundance of massive PBHs. The common definition of strong lensing refers to images with a magnification ratio $R_{\text{f}} = 7$, our $R_{\text{max},\text{f}} = 40$ magnification ratio corresponds to a configuration with a larger impact parameter and hence the lensing optical depth (cross section)

is almost 5 times larger than that normally assumed for lensing calculations. Each source is observed with an approximately fixed angular resolution corresponding to the minimum image separation, $\delta = 0.2$ mas, and limited FoV, $\Delta = 50$ mas. The angular resolution and the limited FoV act to truncate the mass range of the lenses that produce detectable multiple images. Our search is sensitive to the mass range from $\sim 10^4 M_{\odot}$ to $\sim 10^8 M_{\odot}$. In addition, within this lens mass range, the null search result of lensed CRSs leads to a constraint on the upper limit of f_{PBH} . As shown in Fig. 3, at the 68% confidence level, the fraction of DM in the form of massive PBHs with the mass ranging from $10^4 M_{\odot}$ to $10^8 M_{\odot}$ is $\lesssim 0.56\%$. Compared with the limits presented in [Wilkinson et al. \(2001\)](#), our constraint has been significantly improved quantitatively and qualitatively. The quantitative improvement arises from the optical-depth method and the sample consisting of more sources (543, cf. 300). The qualitative improvement is that we use the standard Planck best-fit Λ CDM model, in contrast of the Einstein-de Sitter universe ($\Omega_{\text{M}} = 1, \Omega_{\Lambda} = 0$) used in [Wilkinson et al. \(2001\)](#). These improved constraints would be helpful and complementary for probing the possibility of massive PBHs in this mass window making up DM.

However, the weaker components are so close to the bright cores that it is difficult to study their spectra, polarization, and variability properties. Therefore, we use an effective angular resolution of 2δ as discussed in [Kassiola et al. \(1991\)](#) to compare with the constraints of angular resolution δ . As shown in Fig. 3, the fraction of DM in the form of massive PBHs with the mass ranging from $10^5 M_{\odot}$ to $10^8 M_{\odot}$ is $\lesssim 0.56\%$ at the 68% confidence level. The upper limit of the abundance of massive PBHs is insensitive to the angular resolution δ . This inference is similar as the one concluded in [Kassiola et al. \(1991\)](#). If there is no truncation on mass, the comoving number density n of PBH with a particular mass is proportional to $1/M_{\text{PBH}}$ for a given value of f_{PBH} . In addition, the gravitational lensing cross section σ is $\propto M_{\text{PBH}}$, and hence the path length to lensing $1/(n\sigma)$ is independent on the lens mass. Thus, the optical depth across the measurable mass range is roughly a constant, yielding a universal upper limit of f_{PBH} .

4. CONCLUSIONS AND DISCUSSIONS

In this paper, we have proposed to probe the presence of intergalactic PBHs in the mass range $\sim 10^2 - 10^9 M_{\odot}$ with the lensing effect of CRS which are observed by VLBI with extremely high angular resolution. By searching examples of multiple imaging produced by millilensing in a sample of well-measured 543 CRSs, no

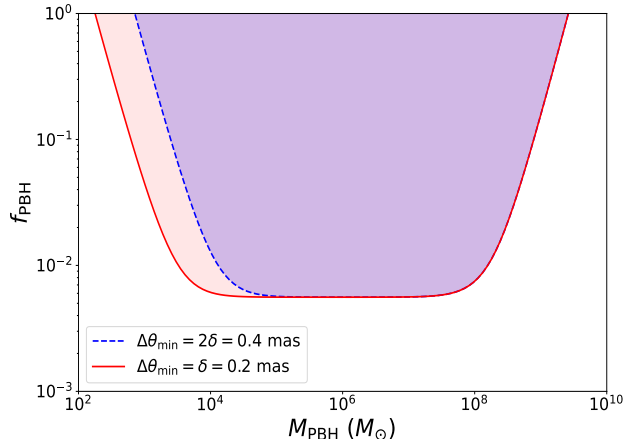


Figure 3. Constraint on f_{PBH} at the 68% confidence level from the null search result of lensing candidate with image separations in the range 0.2(0.4)-50 mas in the well-measured 543 CRSs. The maximum magnifications ratio of the images is $R_{f,\text{max}} = 40$.

evidence of lensed candidates was found with angular separations in the range 0.2-50 milliarcseconds. Based on the optical depth method search result, we derive the 68% confidence-level constraint on the fractional abundance of massive PBHs, $f_{\text{PBH}} < 0.56\%$, in the mass range $\sim 10^4 - 10^8 M_{\odot}$. This constraint might be conservative, because gravitational lensing effect increases the observed flux density of a background source and, as a result, lensed sources are drawn from a fainter source population than the unlensed sources. In this case, a flux-limited survey will probably contain more lensed candidates than expected. Therefore, the null search result formally leads to a more stringent bound on f_{PBH} . This “magnification bias” associated with sources used in our analysis is of order unity. Following [Wilkinson et al. \(2001\)](#), we have neglected this effect.

We expect the constraint on f_{PBH} to be significantly improved in the near future. Assuming detection of $\sim 10^4$ non-lensed CRSs with same redshift distribution, angular resolution and FoV ², we find that uni-

formly distributed massive PBHs in the mass range from $\sim 10^4 M_{\odot}$ to $\sim 10^8 M_{\odot}$ do not make up more than $\sim 0.03\%$ of DM at the 68% confidence level.

The above direct constraints on massive PBH can provide clues about the origin of SMBHs. It is well known that the formation of BHs with masses greater than $\sim 10^9 M_{\odot}$ observed at $z \geq 6$ is still mysterious since the continuous Eddington-limited accretion is far insufficient for stellar-mass black holes growing to SMBHs during the life-time of the universe. PBHs have been widely proposed as seeds of SMBHs. Therefore, direct constraints from the well-measured 543 CRSs would be helpful for exploring this issue. Moreover, supermassive PBHs can form binaries, coalesce, and produce GWs in nano-Hertz frequency band, which can be detected by using stable millisecond pulsars ([Jaffe & Backer 2003](#); [Sesana et al. 2008, 2009](#)). The null-detection of GWs by pulsar timing array (PTA) can successfully constrain continuous GWs from individual supermassive binaries black holes ([Zhu et al. 2014](#); [Babak et al. 2016](#); [Aggarwal et al. 2019](#)). It suggests that PTA experiment also is an important tool to constrain SMBHs in the near future. In combination of millilensing of CRSs and measurement of continuous GWs from individual supermassive binaries black holes, it is foreseen that upcoming complementary multi-messenger observations will yield considerable constraints on the possibilities of massive PBHs.

5. ACKNOWLEDGEMENTS

This work was supported by the National Natural Science Foundation of China under Grants Nos. 11920101003, 11722324, 11603003, 11633001, 12073088, and U1831122; National Key R&D Program of China No. 2017YFA0402600; Guangdong Major Project of Basic and Applied Basic Research (Grant No. 2019B030302001); the Strategic Priority Research Program of the Chinese Academy of Sciences, Grant No. XDB23040100, and the Interdiscipline Research Funds of Beijing Normal University.

REFERENCES

- Abbott, B. P., Abbott, R., Abbott, T. D., et al. 2016, PRL, 116, 061102
- Aggarwal, K., Arzoumanian, Z., Baker, P. T. et al. 2019, ApJ, 880, 116
- Aghanim, N., Akrami, Y., Ashdown, M., et al., 2020, A&A 641, A6
- Alcock, C., Allsman, R. A., Alves, D. R., et al. 2001, ApJ, 550, L169
- Ali-Haïmoud Y., Kamionkowski M. 2017, PRD, 95, 043534
- Aloni, D., Blum, K., & Flauger, R. 2017, JCAP, 1705, 017
- Ashoorioon, A., Rostami, A., & Firouzjaee, J. T. 2019, arxiv:1912.13326
- ² http://www.gaoran.ru/english/as/ac_vlbi/

- Babak, S., Petiteau, A., Sesana, A., et al. 2015, *MNRAS*, 455, 1065
- Bernal, J. L., Bellomo, N., Raccanelli, A., & Verde, L. 2017, *JCAP*, 10, 052
- Bird, S., Cholis, I., Muñoz, J. B., Ali-Haïmoud, Y., & Kamionkowski, M. 2016, *PRL*, 116, 201301
- Blandford, R. D., & Königl, A. 1979, *ApJ*, 232, 34
- Brandt, T. D. 2016, *ApJ*, 824, L31
- Caldwell, R. R., Chamblin, A., & Gibbons, G. W. 1996, *PRD*, 53 7103
- Cao, S., Biesiada, M., Gavazzi, R., Piórkowska, A., & Zhu, Z.-H. 2015, *ApJ*, 806, 66
- Cao, S., Biesiada, M., Jackson, J., Zheng, X.-G., & Zhao, Y.-H. 2017a, *JCAP*, 02, 012
- Cao, S., Zheng, X.-G., Biesiada, M., et al. 2017b, *A&A*, 606, A15
- Cao, S., Biesiada, M., Qi, J.-Z., et al. 2018, *EPJC*, 78, 749
- Carr, B. J., & Hawking, S. W. 1974, *MNRAS*, 168, 399
- Carr, B. J. 1975, *ApJ*, 201, 1
- Carr, B. J., & Lidsey, J. E. 1993, *PRD*, 48, 543
- Carr, B. J., Gilbert, J. H., & Lidsey, J. E. 1994, *PRD*, 50, 4853
- Carr, B. J., Kohri, K., Sendouda, Y., & Yokoyama, J. 2016, *PRD*, 94, 044029
- Chen, L., Huang, Q.-G., & Wang, K. 2016, *JCAP*, 1612, 044
- Chen, C., & Cai, Y.-F. 2019, *JCAP*, 10, 068
- Chen, Z.-C., Yuan, C., & Huang, Q.-G. 2020, *PRL*, 124, 251101
- Chen, Z.-C., & Huang, Q.-G. 2020, *JCAP*, 08, 039
- Clark, S., Dutta, B., Gao, Y., Ma, Y.-Z., & Strigari, L. E. 2018, *PRD*, 98, 043006
- Clesse, S., & García-Bellido, J. 2015, *PRD*, 92, 023524
- Clesse, S., & García-Bellido, J. 2017a, *Phys. Dark Univ.* 15, 142
- Clesse, S., & García-Bellido, J. 2017b, *Phys. Dark Univ.* 18, 105
- De Luca, V., Franciolini, G., Pani, P., & Riotto, A. 2020, *JCAP*, 06, 044
- DeRocco, W., & Graham, P. W. 2019, *PRL*, 123, 251102
- Diego, J. M. 2020, *PRD*, 101, 123512
- Duechting, N., 2004, *PRD*, 70, 064015
- Fu, C.-J., Wu, P.-X., & Yu, H.-W. 2019, *PRD*, 100, 063532
- Gert, H., Martti, R., Ville, V., & Hardi, V. 2020, *arXiv:2012.02786*
- Graham, P. W., Rajendran, S., & Varela, J. 2015, *PRD*, 92, 063007
- Green, A. M., & Kavanagh, B. J. 2020, *arXiv:2007.10722*
- Griest, K., Cieplak, A. M., & Lehner, M. J. *PRL*, 111, 181302
- Gurvits, L. I., 1994, *ApJ*, 425, 442
- Gurvits, L. I., Kellerman, K. I., & Frey, S. 1999, *A&A*, 342, 378
- Halder, A., & Banerjee, S. 2020, *arXiv:2102.00959*
- Hasegawa, F., and Kawasaki, M., 2018, *PRD*, 98, 043514
- Hawking, S. W. 1971, *MNRAS*, 152, 75.
- Hawking, S. W., Moss, I. G., & Stewart, J. M. 1982, *PRD*, 26, 2681
- Hawking, S. W. 1989, *PLB*, 231, 237
- Hektor, A., Hutsi, G., Marzola, L., Raidal, M., Vaskonen, V., & Veermae, H. 2018, *PRD*, 98, 023503
- Hogan, C. J. 1984, *PLB*, 143, 87
- Huang, Z. 2019, *PRD*, 99, 103537
- Jackson, J. C. 2004, *JCAP*, 11, 7
- Jackson, J. C., & Jannetta, A. L. 2006, *JCAP*, 11, 002
- Jackson, J. C. 2012, *MNRAS*, 426, 779
- Jaffe, A. H., & Backer, D. C. 2003, *ApJ*, 583, 616
- Ji, L., Kovetz, E. D., & Kamionkowski, M. 2018, *PRD*, 98, 123523
- Kassiola, A., Kovner, I., & Blandford, B. D. 1991, *ApJ*, 358, 5
- Kawasaki, M., Kusenko, A., and Yanagida, T. T., 2012, *PLB*, 711, 1
- Kawasaki, M., and Murai, K., 2019, *PRD*, 100, 103521
- Kellermann, K. I. 1993, *Nature*, 361, 134
- Kitajima, N., and Takahashi, F., 2020, *JCAP*, 11, 060,
- Kohri, K., Nakama, T., & Suyama, T. 2014, *PRD*, 90, 083514
- Koushiappas, S. M., & Loeb, A. 2017, *PRL*, 119, 041102
- Kovalev, Y. Y., et al., 2005, *AJ*, 130, 2473
- Laha, R. 2019, *PRL*, 123, 251101
- Laha, R., Muñoz, J. B., & Slatyer, T. R. 2020, *PRD*, 101, 123514
- Liao, K., Zhang, S.-B., Li, Z., & Gao, H. 2020, *ApJL*, 896, L11
- Liao, K., Tian, S.-X., & Ding, X.-H. 2020, *MNRAS*, 495, 2002
- Lobanov, A. P. 2005, *A&A*, *arXiv:0503225*
- Mediavilla, E., Jimenez-Vicente, J., Munoz, J. A., VivesArias, H., & Calderon-Infante, J. 2017, *ApJ*, 836, L18
- Motohashi, H., Mukohyama, S., & Oliosi, M. 2020, *JCAP*, 03, 002
- Nakama, T., Suyama, T., & Yokoyama, J. 2016, *PRD*, 94, 103522
- Niikura, H., Masahiro, T., Naoki, Y., et al. 2019, *Nature Astronomy*, 3, 524.
- Niikura, H., Takada, M., Yokoyama, S., Sumi, T., & Masaki, S. 2019, *PRD*, 99, 083503
- Nemiroff, R. J. 1989, *ApJ*, 341, 579

- Pi, S., Zhang, Y.-L., Huang, Q.-G., and Sasaki, M. 2018, JCPA, 1805, 42
- Poulin, V., Serpico, P. D., Calore, F., Clesse, S., & Kohri, K. 2017, PRD, 96, 083524
- Preston, R. A., Morabito D. D., Williams J. G., et al. 1985, AJ, 90, 1599
- Qi, J.-Z., Cao, S., Zhang, S.-X., et al. 2019, MNRAS, 483, 1104
- Qi, J.-Z., Zhao, J.-W., Cao, S., Biesiada, M., & Liu, Y.-T. 2021, MNRAS, 503, 2179
- Sasaki, M., Suyama, T., Tanaka, T., and Yokoyama, S., 2016, PRL, 117, 061101
- Sasaki, M., Suyama, T., Tanaka, T., & Yokoyama, S. 2018, GReGr, 35, 063001
- Sesana, A., Vecchio, A., & Colacino, C. N. 2008, MNRAS, 390, 192
- Sesana, A., Vecchio, A., & Volonteri, M. 2009, MNRAS, 394, 2255
- Shinohara, T., Suyama, T., & Takahashi, T. 2020, arXiv:2103.13692
- Tisserand, P., Guillou, P., Afonso, C., et al, 2007, A&A 469, 387
- Wang, S., Wang, Y.-F., Huang, Q.-G., & Li, T. G. F. 2018, PRL, 120, 191102
- Wilkinson, P. N., Henstock, D. R., Browne, W. A., et al. 2001, PRL, 86, 4
- Woods, T. E., Agarwal, B., Bromm, V., et al. 2019, PASA, 36, e027
- Yang, J., Wang, F., Fan, X., et al. 2020, ApJ, 897, L14
- Zhou, H., Li, Z.-X., Gao, H., & Huang, Z.-Q. 2021, arxiv:2103.08510
- Zhu, X.-J., Hobbs, G., Wen, L. et al. 2014, MNRAS, 444, 3709
- Zumalacarregui, M., & Seljak, U. 2018, PRL, 121, 141101